

Effect of air jet vortex generators on a shock wave boundary layer interaction

L. J. Souverein · J.-F. Debiève

Received: 20 August 2009/Revised: 17 February 2010/Accepted: 22 February 2010/Published online: 10 March 2010
© The Author(s) 2010. This article is published with open access at Springerlink.com

Abstract The effect of upstream injection by means of continuous air jet vortex generators (AJVGs) on a shock wave turbulent boundary layer interaction is experimentally investigated. The baseline interaction is of the impinging type, with a flow deflection angle of 9.5° and a Mach number $M_e = 2.3$. Considered are the effects of the AJVGs on the upstream boundary layer flow topology and on the spatial and dynamical characteristics of the interaction. To this aim, Stereoscopic Particle Image Velocimetry has been employed, in addition to hot-wire anemometry (HWA) for the investigation of the unsteady characteristics of the reflected shock. The AJVGs cause a reduction of the separation bubble length and height. In addition, the energetic frequency range of the reflected shock is increased by approximately 50%, which is in qualitative agreement with the smaller separation bubble size.

1 Introduction

The effect of a planar shock impinging on a turbulent boundary layer establishes one of the classic interaction phenomena in compressible viscous flow analysis. This particular form of interaction also has a direct technological relevance to the performance of high-speed vehicles,

affecting for example the efficiency of supersonic intakes and rocket engine nozzles. Furthermore, maximum mean and fluctuating pressure and thermal loads on a structure are most often found in regions of shock wave boundary layer interaction (SWBLI) and are thus important design factors. Flow control is seen as an important issue in future vehicle developments to negate these adverse effects (Dolling 2001).

Boundary layer separation can occur, provided that a sufficiently strong adverse pressure gradient is imposed by the shock system. The resulting bubble of reversed flow has been observed to pulse, leading to low-frequency oscillations of the reflected shock, causing detrimental unsteady fluctuations. The unsteadiness produced exhibits a wide range of spatial and temporal scales. The reflected shock foot unsteadiness shows frequencies that are about two orders of magnitude lower than the incoming boundary layer frequency U_e/δ_0 , where U_e is the free-stream velocity and δ_0 is the boundary layer thickness. One of the open issues is the source of the pulsation. Two principal mechanisms have been proposed, ascribing the unsteadiness either to large-scale elongated structures in the upstream boundary layer (see for example Beresh et al. 2002; Ganapathisubramani et al. 2007; Humble et al. 2009; Souverein et al. 2009), or to a mechanism based on the entrainment of mass by the shedding of large-scale coherent structures (see Piponnier et al. 2009; Souverein et al. 2009).

Various systems have been imagined to control the interaction, the objective being either to reduce the shock strength with the aim of reducing the drag or to reduce the extent of the flow separation in order to suppress the unsteadiness, or both, see Délerly 2000. Considering the first approach, examples are found in the studies by Bur et al. 1997 and Doerffer and Szluc 2002. Considering the second objective, various systems have been imagined.

L. J. Souverein · J.-F. Debiève
Institut Universitaire des Systèmes Thermiques Industriels,
Supersonic Group, 5 rue Enrico Fermi,
13453 Marseille Cedex 13, France

L. J. Souverein (✉)
Faculty of Aerospace Engineering,
Delft University of Technology, Kluyverweg 1,
2629 HS, Delft, The Netherlands
e-mail: l.j.souveirin@tudelft.nl

The most sophisticated concern the dynamic control using actuators in a feedback loop, some time dependent actuation, or a combination of multiple control methods (see for example Selig and Smits 1991; Bueno et al. 2003; Bueno et al. 2006; Valdivia et al. 2009). More crude solutions consist of static systems based on the generation of vortices near the wall upstream of the interaction. One can think of sub-boundary layer vortex generators, consisting of mechanical devices fixed at the wall (see for example Ashill et al. 2001; Bueno et al. 2006; Holden and Babinsky 2007; Bruce and Babinsky 2008; Blinde et al. 2009; Lee et al. 2009; Lee and Loth 2009; Bur et al. 2009). A review of different types of such mechanical control devices and their effectiveness is given by Lin 2002. An alternative control method is based on the injection, suction, or bleed of fluid (see Viswanath 1988 for an overview of different approaches and their effectiveness). This approach is of particular interest due to the potential of integrating flow control with transpiration cooling, see Kamotani and Greber 1972. The purpose of the current work is to experimentally investigate the effectiveness of control through fluid injection by means of an array of continuous air jet vortex generators (AJVGs) in the upstream boundary layer. This is done in the fully supersonic flow domain at a Mach number of 2.3.

The aim of the current investigation is to modify the mean inflow boundary layer through a static control approach in an attempt to alter the size of the mean separation bubble, and to characterise the consequences of this change in mean flow organisation on the shock unsteadiness. From this vantage point, the effect of continuous air jet vortex generators on a shock wave turbulent boundary layer interaction is experimentally investigated in the case of a supersonic flow with a Mach number of $M_e = 2.3$. The associated flow deflection angle is 9.5° , leading to a significant mean separation bubble for the baseline interaction. In the first place, the influence of the air jet vortex generators on the incoming boundary layer and the subsequent modification of the separation bubble topology are examined. Secondly, the unsteady aspects and the resulting modification of the shock dynamics are investigated.

2 Experimental arrangement and flow conditions

The experiments have been performed in the S8 supersonic wind tunnel at the Institut Universitaire des Systèmes Thermiques Industriels (IUSTI) in Marseille. The tunnel has been equipped with a special measurement section to perform the experiments with air jet vortex generator control. The flow conditions and the set-up of the control experiment are detailed in the following.

2.1 Flow facility

The wind tunnel is a closed-loop continuously running facility with a particularly low free-stream turbulence level ($\rho u'/\rho u = 0.002$, see Souverein et al. 2008). The Mach number is $M_e = 2.3$ (with a variation of 0.6% over an upstream distance of 0.2 m), the stagnation temperature is $T_0 = 295$ K (with a variation of <0.5 K/h), and the total pressure is $p_0 = 0.5$ atm (it is controlled to within an accuracy of 0.02%). The inlet conditions for the interaction are a unit Reynolds number $5.5 \times 10^6 \text{ m}^{-1}$, a Reynolds number based on compressible momentum thickness of approximately $Re_\theta = 5,000$, a friction coefficient of $C_f = 2.1 \times 10^{-3}$, and a boundary layer thickness of $\delta_0 \approx 10$ mm ($99\%U_e$). An extensive description of the flow facility can be found in (Dupont et al. 2005 and Dupont et al. 2008).

2.2 Control experiment set-up

A row of air jet vortex generators (AJVGs) has been placed upstream of the interaction to study the effect of upstream disturbances on the mean and unsteady flow characteristics for the control of a shock wave boundary layer interaction (SWBLI), see Fig. 1. The vortex generator array consists of a row of ten holes, with a spanwise pitch of about one boundary layer thickness. The diameter of the holes is $\phi = 0.8$ mm ($\phi < \delta/10$). The array is oriented perpendicular to the free-stream flow direction. The axis of the holes is inclined within the spanwise-wall-normal plane at an angle of $\psi = 45^\circ$. The AJVG array has been located at around $5\delta_0$ upstream of the zone of the reflected shock oscillations and 124.5 mm upstream of the extrapolated wall impact point of the incident shock. A settling chamber is installed underneath the complete array of AJVGs to assure homogeneous and stable air injection. For practical reasons, the stagnation pressure in the chamber is chosen at $P_{0\text{jets}} = 0.4$ bar, close to the stagnation pressure of the tunnel ($p_0 = 0.5$ atm). Varying the injection pressure showed that a lower pressure will lead to a smaller effect on the interaction. The temperature in the chamber is around the stagnation temperature of the channel flow. Assuming that the flow conditions at the injection orifices are critical, a jet injection velocity of $V_{\text{jet}} = 314$ m/s is obtained. It was verified that the pressure spectrum in the chamber, which has been filled with a porous medium, does not present any resonant peaks. The current experimental set-up constitutes a first attempt of AJVG control to investigate the effect on the mean flow organisation. It can serve as a basis for further parametric optimisation of the jet configuration (injection angle, jet size and spacing, upstream location of the array, injection pressure, etc.).

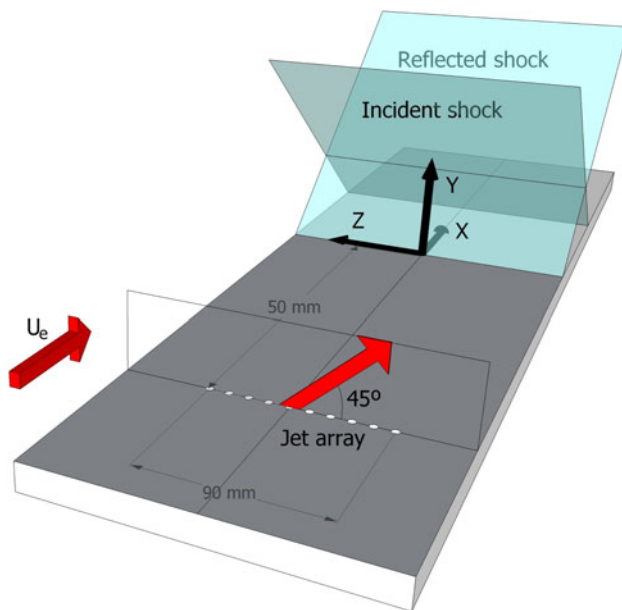


Fig. 1 Schematic representation of the air jet vortex generator experiment set-up

The injected airflow was found to be negligible when compared to the mass flow deficit of the boundary layer: for an injection pressure of $P_{0\text{jets}} = 0.4$ bar, considering the contribution of the row of ten injectors over their span of $\Delta Z = 100$ mm, and given the compressible boundary displacement thickness of $\delta^* = 3$ mm, the ratio of the jet mass flow to the boundary layer mass flow deficit is:

$$\frac{\text{Jet flux}}{\rho_e U_e \delta^* \Delta Z} \approx 3\%$$

2.3 Flow diagnostic methods

For the hot-wire anemometry measurements, the constant temperature system ‘Streamline Dantec CTA’ was used in balanced bridge mode. The diameter of the hot wire is $5 \mu\text{m}$, and the overheat ratio was 0.6. The data were sampled with a National Instruments recorder NI6133 using approximately 2×10^6 samples.

The PIV investigation was made using a Dantec Dynamics system and software. The light sheets are generated by a double pulse ND:YAG laser New Wave Solo II, which delivers 30 mJ per pulse, with a pulse delay set in the range of 1–2 μs . The light sheet thickness is approximately 0.5 mm. Incense smoke was used to seed the boundary layer. The particles were injected from the wall, upstream of the wind tunnel nozzle. The time constant of the particles was estimated to be 4.5 μs , corresponding to a diameter of 0.5 μm , (Elena et al. 1999). The particle images are recorded by Flowsense 10-bit cameras with a CCD size of $1,600 \times 1,200$ pixels, equipped with Nikon Macro Nikkor $f = 60$ mm $f/2.8$ objectives with the

diaphragm set to $f\# = 2.8$. The acquisitions were made using Flowmanager 4.71 software via the Dantec Flowmap System Hub. A peculiarity of this system is an internal storage, and therefore long data acquisitions at high rate are possible (12 Hz using the two cameras in half frame mode). A maximum of 10,000 image pairs were acquired with two cameras (5,000 per camera). The images were processed with DynamicStudio2.00; statistics and post-processing were done with in-house Matlab routines.

The PIV analysis consist of an iterative cross-correlation of the image pairs using an interrogation window size of 64×32 pixels and a single iteration step giving a final size of 32×16 pixels. A Gaussian weighting function was applied to the iteration windows, giving a final effective window size of 16×8 pixels. Three iterations were performed on the final window size to refine the result. An overlap factor of 75% was employed. Within the iterative process, the data were validated employing several criteria (peak width, peak height, local neighbourhood median filter). It was verified that sufficient particle images were present within the final effective iteration windows. The correlation and validation settings were optimised to obtain consistent results in combination with a high validation rate within regions of large velocity gradients (notably the reflected shock foot). Before analysing the images, a minimum background intensity was subtracted. The background was obtained per batch of 500 images to compensate for possible variations in intensity during the course of the run.

Two distinct PIV experiments were performed. In the first place, measurements were made in the wall parallel plane using a stereoscopic PIV system. In the second place, acquisitions were made in the streamwise-wall-normal plane using a 2C-PIV system with two side by side cameras in panoramic mode.

In the first place, the horizontal plane stereo-PIV measurements were made using the full CCD size. A maximum number of 3,500 acquisitions (7,000 image pairs) were made per run, consisting of 500 reference measurements without AJVGs and 3,000 measurements with AJVGs. The final field of view was approximately $100 \times 100 \text{ mm}^2$ ($10\delta_0 \times 10\delta_0$), and the magnification factor in the de-warped images was 10.0 pix/mm (note that in the actual acquisitions, the scale factor depends on the location within the image due to perspective effects; the value is hence indicative). A pulse separation of 2 μs was employed, yielding a free-stream displacement of 11 pixels and a displacement of 7.2 pixels at 1 mm height from the wall. The final PIV resolution is $0.60 \times 0.62 \text{ mm}^2$, yielding a field of 250×249 vectors. Two domains of interest were considered: the incoming boundary layer and the interaction, covering a total streamwise distance of approximately $20\delta_0$.

In the second place, the vertical plane panoramic 2C-PIV measurements were made using two cameras mounted side by side to obtain a panoramic field of view. Each CCD was cropped to a size of $1,600 \times 595$ pixels. The number of acquisitions was between 2,000 and 5,500 per run, of which 500 were reference measurements without AJVGs, and the rest were with AJVGs. The images from each camera were stitched together to obtain an effective sensor size of $3,018 \times 595$ pixels. The final field of view was $224 \times 44 \text{ mm}^2$ with a magnification factor of 13.5 pix/mm. A pulse separation of $1 \mu\text{s}$ was employed, yielding a free-stream displacement of 7.4 pixels. The final PIV data resolution is $0.58 \times 0.29 \text{ mm/vect}$, yielding a field of 374×77 vectors. The useful data range is $224 \times 20 \text{ mm}^2$ (approximately $22\delta_0 \times 2\delta_0$). The jet velocity in the vicinity of the jet exit at the wall ($\phi = 0.8 \text{ mm}$) was not characterised; the air jets themselves are not seeded and the PIV resolution is insufficient for this purpose.

Concerning the experimental accuracy of the PIV measurements, different types of uncertainties have to be taken into account. Amongst others, one can consider the PIV measurement resolution on the instantaneous realisations, which is generally assumed to be 0.1 pixel (corresponding to around 1% of the free-stream velocity), see Scarano and Riethmuller 1999. Furthermore, given the large ensemble sizes, the statistical convergence errors are expected to be at most of the same order (1% of the free-stream velocity or less). More relevant for the PIV measurement accuracy, and more difficult to predict, are bias errors, cause by for example peak locking. To ascertain the quality of the PIV data, a cross-verification has been made with LDA measurements, yielding consistent results (see Dupont et al. 2008).

The measurement programme and the data field resolution are summarised in Table 1. The measurement plane locations refer to the height (h) or span wise location with respect to the tunnel axis (z) for the 3C-PIV and 2C-PIV experiments, respectively. The ensemble size indicates the number of acquired realisations with AJVGs on and off, respectively. Either the spanwise or the wall

normal resolution within the measurement plane is given, depending on the experiment.

2.4 General description of the flow

The flow topology is depicted in Fig. 2, showing a Schlieren visualisation of the interaction with and without control. As can be observed, the fully turbulent boundary layer which develops on the tunnel floor is subjected to a shock wave produced by a full-span sharp edge plate placed in the external flow. The imposed flow deflection angle is 9.5° , corresponding to a well-developed separation. The baseline interaction has been extensively documented in literature (Dupont et al. 2005, 2006, 2008; Dussauge and Piponniau 2008). As will appear from Fig. 9, this interaction is three-dimensional in nature. This is a known fact for interactions at high incidence angle, as has been shown in literature by means of surface flow visualisations, see for example Green 1970. The three-dimensional aspects of this interaction have been investigated in detail in Dussauge et al. 2006, where the existence of two counter-rotating tornado-like vortices has been put in evidence within the interaction region.

As can be observed, the boundary layer is first perturbed by the AJVG array, which is located at the source of the weak shock-expansion system located upstream of the interaction. The free-stream velocity downstream of the jets has been verified to be identical to the undisturbed upstream value. Approximately $5\delta_0$ downstream of the AJVG array, the incident shock wave impacts on the boundary layer, causing the boundary layer to thicken and to separate. The jets cause a thickening of the reflected shock, indicative of either an increased unsteadiness (shock excursion amplitude) or an increase in three-dimensionality (due to spanwise rippling). As can be observed, the interaction length (distance at the wall between the extrapolated incident and reflected shock) is not significantly affected.

The associated mean streamwise velocity is presented in Fig. 3. The flow is from left to right, showing the undisturbed incoming boundary layer on the left-hand side of the domain of interest. As can be seen, the boundary layer is perturbed by the jet array at $X = 212.5 \text{ mm}$. The boundary layer thickens, but without a change in free-stream velocity. The reflected shock foot is located at approximately $X = 270 \text{ mm}$, where the flow is lifted away from the wall and a separation bubble appears. The solid black contour line indicates the contour of zero velocity. The dashed contour represents the extent of the zero velocity contour for the undisturbed case. The dashed line indicates the extrapolated incident shock, impacting at $X = 337 \text{ mm}$. As can be observed, the jets significantly decrease the separation bubble size. In the following sections, the effect of the jets will be quantified in more detail.

Table 1 Measurement parameters

Parameter		3C-PIV	2C-PIV
Measurement plane	$h; z$ [mm]	1, 2, 4, 6	-2.5, -5, 0, 2.5
Ensemble size	AJVGs on/off	500/3500	500/1500–5000
Data resolution	$\Delta X/\delta_0$	60×10^{-3}	58×10^{-3}
	$\Delta Z/\delta_0; \Delta Y/\delta_0$	62×10^{-3}	29×10^{-3}
	ΔX^+	45	44
	$\Delta Z^+; \Delta Y^+$	47	22

Fig. 2 Schlieren visualisation of the interaction; *left*: baseline interaction without AJVGs; *right*: modified interaction with AJVGs

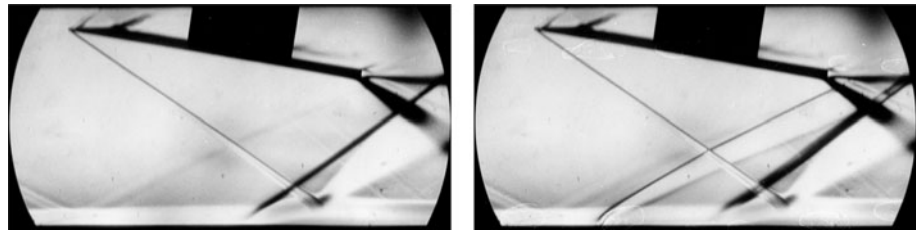
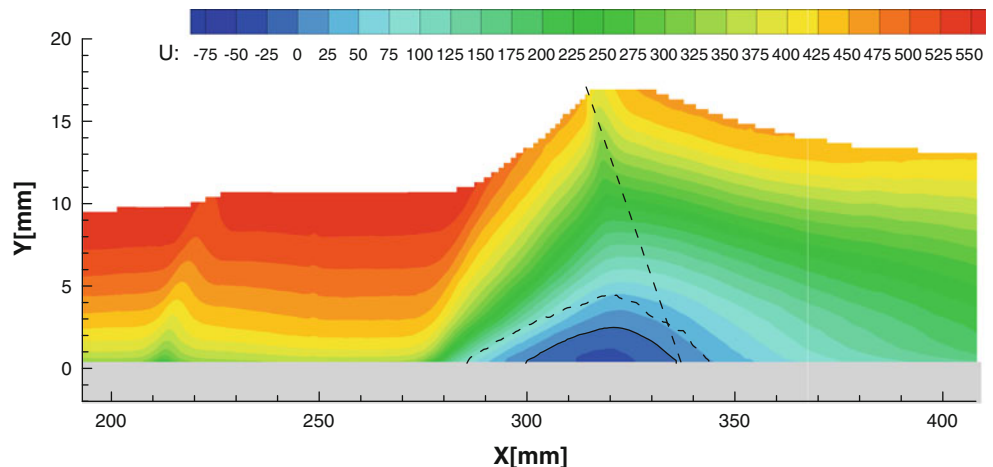


Fig. 3 Mean longitudinal velocity component (m/s) in the streamwise-wall-normal plane with the minimum interaction length ($Z = 2.5$ mm), AJVGs on. The *solid contour line* indicates the extent of the separation bubble with AJVGs. The *dashed contour line* shows the bubble size without AJVGs



3 Air injection influence on the interaction

This chapter treats in detail the effect of the air jet vortex generators on the flow organisation. First, the modification of the upstream boundary layer is considered, secondly the change in the separation bubble topology characterised, and finally the effect on the shock unsteadiness is investigated.

3.1 Modification of the upstream boundary layer

To quantify the effect of the jets on the incoming boundary layer topology, three-component PIV measurements have been made in the horizontal plane at four heights. The modification of the three velocity components (U, V and W) in the upstream boundary layer is shown in Fig. 4. Compared are the spanwise profiles with and without AJVGs for the four measurement plane heights. As can be observed, the jets induce a strong spanwise periodic modulation of the velocity. The modulation in the U -component has an amplitude of 5% (min–max variation of 10%) of the free-stream velocity at $h = 2$ –4 mm. The effect of the jets is to locally increase the velocity close to the wall, while at the same time causing an overall decrease in the velocity higher up in the boundary layer. Without AJVGs, there remains a small undulation in the velocity in the boundary layer. This velocity variation, which is in the range of $1\%U_e$, is of the order as the measurement accuracy and it has been attributed to Görtler vortices, see Dussauge and

Piponniau (2008). Considering the wall normal and spanwise components (V and W respectively), a modulation with the same wavelength is observed, but of a smaller amplitude (2% of the free-stream velocity). In addition, a consistent bias is introduced in the W -component due to the blowing direction of the jets, inducing a spanwise skewing of the flow.

The spanwise wall parallel measurements from the four measurement planes enable the visualisation of the flow field through a reconstruction of the mean three-dimensional velocity data, encompassing the complete domain of interest from the incoming boundary layer up to reattachment. For this data volume, the angular velocity around the local velocity vector has been computed. Figure 5 shows the resulting iso-surfaces for values of -5×10^3 rad/s and 5×10^3 rad/s superimposed on a contour map of the streamwise mean velocity component at a height of $Y = 1$ mm.

As a first observation it is noted that the jets induce a spanwise asymmetry, as already indicated by Fig. 4, skewing the flow with a small angle of approximately 2.8° with respect to the tunnel axis. Secondly, the flow is modulated in the spanwise direction. Pairs of counter-rotating longitudinal vortices, which are induced by each jet, are at the origin of this spanwise modulation. The blue angular velocity iso-surfaces show the main vortices produced by the AJVGs, having negative angular velocity values (turning counter-clockwise (CCW) when looking downstream along the coordinate axis). Also visible are (in

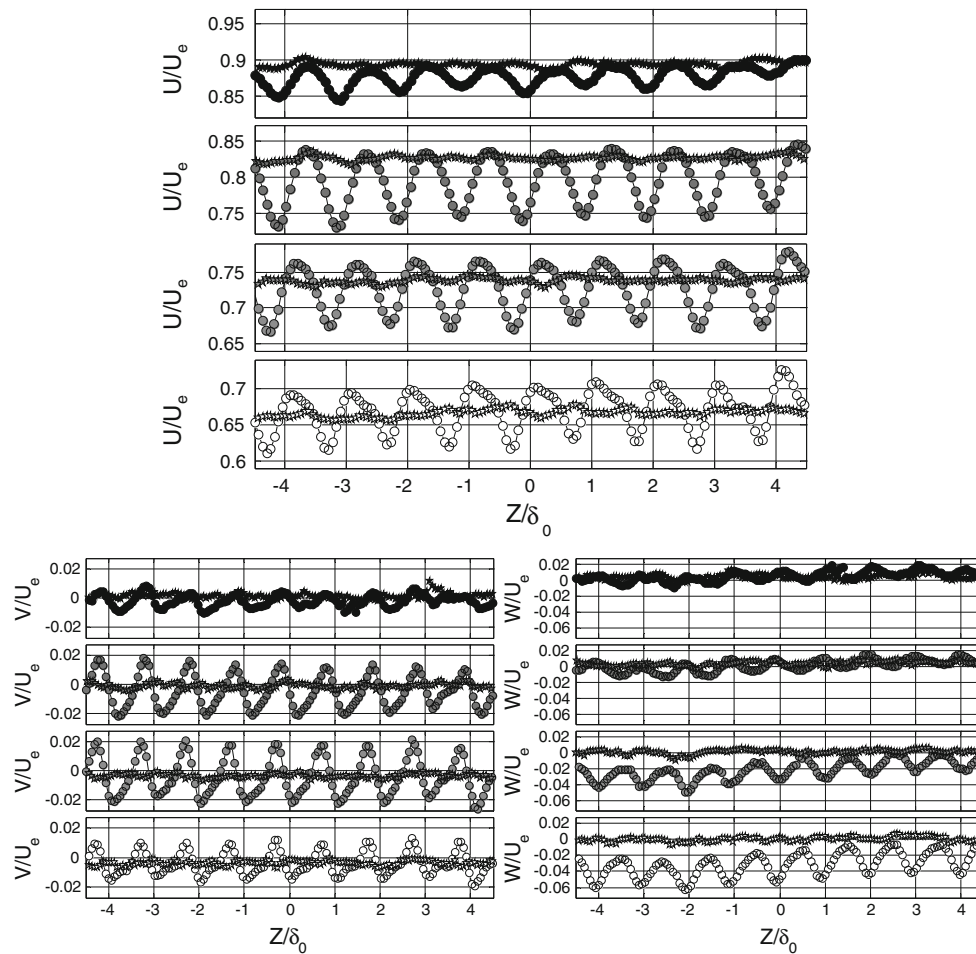
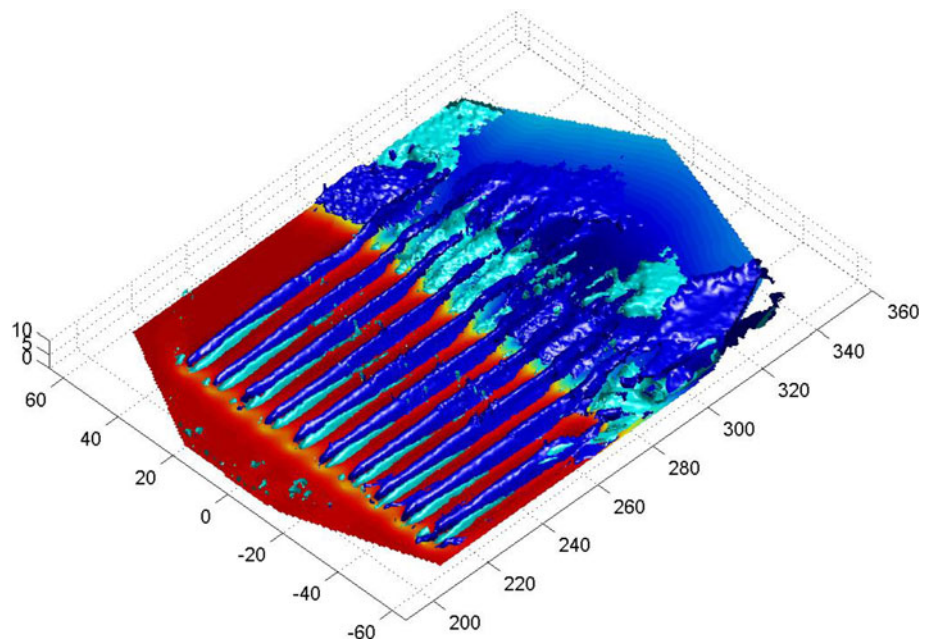


Fig. 4 Spanwise distributions of the U, V and W velocity components compared with and without AJVGs. Profiles taken at $X = 260$ mm for the four measurement planes ($h = 1, 2, 4$ and 6 mm). Grey levels indicate the measurement plane height (white = 1 mm, black = 6 mm)

Fig. 5 Iso-surfaces of the angular velocity (blue: $\alpha = -5 \times 10^3$ rad/s and cyan: $\alpha = 5 \times 10^3$ rad/s), superimposed on contour of the mean longitudinal velocity at $Y = 1$ mm



cyan) small vortex tubes with a positive angular velocity, which turn clockwise (CW) when looking downstream. These correspond to small secondary vortices generated between the jets and the wall (the main vortices are generated between the jets and the outer flow, above the jets).

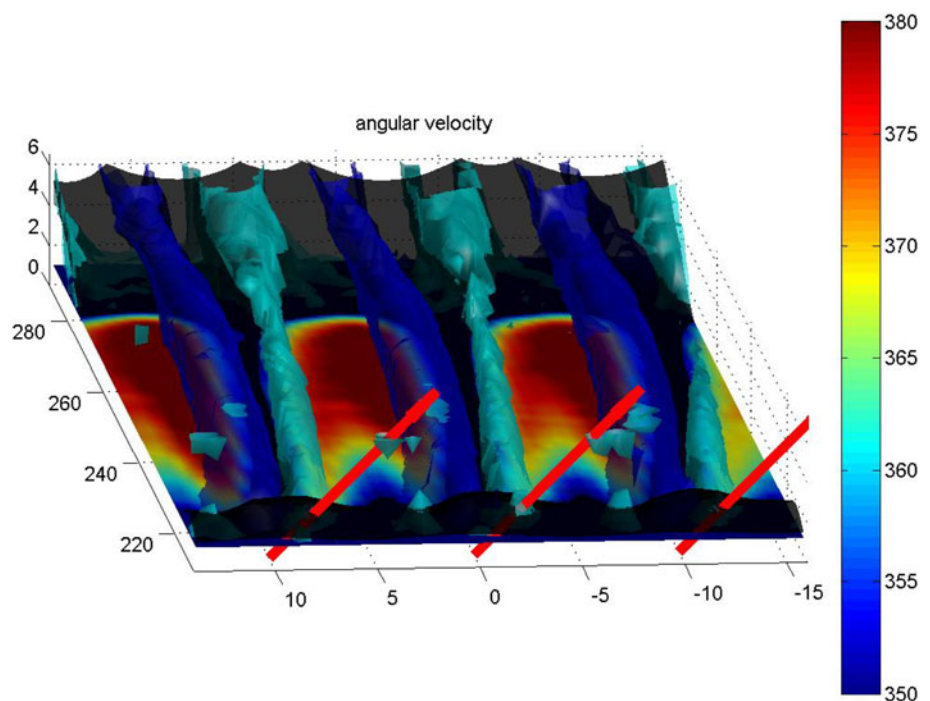
The formation of a symmetrical pair of counter-rotating vortices is a well-documented phenomenon for a jet in crossflow that has been evidenced both experimentally and numerically (see for example Kamotani and Greber 1972; Andreopoulos and Rodi 1984; Fric and Roshko 1994; Smith and Mungal 1998; Cortelezzi and Karagozian 2001). They are formed in the near field, close to the jet, and become dominant in the far field. A schematic of the near field formation of the longitudinal vortices is given by Fric and Roshko 1994. The generation of the vortex pair has been explained theoretically by Broadwell and Breidenthal 1984. They have shown that the counter-rotating vortices find their origin in the jet momentum that is injected into the crossflow, which can be interpreted as a transverse force, in other words ‘lift’. It is this lift force that generates the vortex pair, as in the case of a wing. In the case of inclined jet injection, two asymmetric vortex structures have also been observed both numerically, see Yang and Wang 2005, and experimentally in a low subsonic flow, see Yamagata et al. 2009. The existence of longitudinal vortices has also been shown in experiments and computations with mechanical sub-boundary layer vortex generators (see for example Holden and Babinsky 2007, Blinde et al. 2009; Lee et al. 2009;

Lee and Loth 2009). The numerical results of Lee et al. 2009 show furthermore that the roll-up of such longitudinal vortex structures is also observed instantaneously. The asymmetry in the current experiment appears to be the direct consequence of the inclination of the jet, ‘squeezing’ as it was one of the vortices between the wall and the jet, while reinforcing the vortex on top of the jet.

A zoom of the topology of these vortices is presented in Fig. 6. As can be observed from this figure, the mean velocity in between the jets is increased from $U = 350$ m/s to $U = 380$ m/s, in accordance with Fig. 4. Since the velocity increase is directly associated with the two vortices, it seems to be an induced effect of the rotation of the longitudinal vortex pairs, which transport fluid from higher up in the boundary layer towards the wall. At the same time, the mean velocity behind each jet is reduced, most likely as a result of the transport of low speed fluid away from the wall by the vortices, in combination with the generation of a wake by the jets themselves. The formation of such a wake has been studied in detail for a jet in crossflow by Fric and Roshko (1994).

From the preceding plots, the following vortex structure can be intuited, as illustrated schematically in Fig. 7 (looking in the upstream direction with the negative spanwise coordinate pointing left). Using the following velocities and estimated diameter for the longitudinal vortex, an estimate of the angular velocity for the large CCW vortex at mid-distance between the jets and shock foot can be obtained:

Fig. 6 Iso-surfaces of the angular velocity (blue: $\alpha = -5 \times 10^3$ rad/s and cyan: $\alpha = 1 \times 10^3$ rad/s). Black iso-surface represents longitudinal velocity iso-contours of $U = 350$ m/s (low speed fluid). Contours indicate longitudinal velocities at $Y = 1$ mm in m/s, as indicated by the colour bar on the right. Red arrows represent the jet location and injection direction



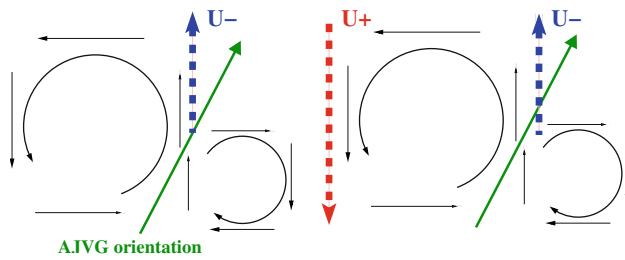


Fig. 7 Schematic representation of the longitudinal vortices generated by the AJVGs, viewed in the upstream direction. The green arrow represents the jet

- diameter: $D = 6$ mm
- mean out of plane velocity: $V = 10$ m/s;
- horizontal velocity component: $W_1 = -30$ m/s (for $Y = 1$ mm);
- $W_4 = 10$ m/s (for $Y = 4$ mm)
- distance from jet to interaction: $L = 50$ mm
- longitudinal velocity: $U_1 = 350$ m/s (for $Y = 1$ mm);
- $U_4 = 430$ m/s (for $Y = 4$ mm)
- rotation rate:

$$\alpha = \frac{W_4 - W_1}{2\pi D} = \frac{40}{2\pi \times 6 \times 10^{-3}} = 1,000 \text{ Hz}$$

$$= 6.7 \times 10^3 \text{ rad/s}$$

This value is in good agreement with the values for the iso-surface for the principal longitudinal vortex in Fig. 7. The travel time from the jets to the interaction can be obtained as follows:

$$\tau = \frac{2L}{U_4 + U_1} = \frac{2 \times 50 \times 10^{-3}}{350 + 430} = 128 \mu\text{s}$$

The number of rotations executed by the large CCW vortex from its generation until the interaction is hence approximately: $\alpha\tau = 0.13$. Performing the same estimation just behind the jet, where the out of plane velocities are stronger, leads to a value of $\alpha\tau = 0.31$. So the total number of rotations may be expected to be around 1/4, certainly less than 1. This means that the mixing induced by the rotation of the longitudinal vortices is limited.

The obtained mean longitudinal velocity profiles at $X = 260$ mm, just upstream of the reflected shock foot, are visualised in Fig. 8. Shown are the profile for the reference case without jets (L_{ref} , shown in black) and two profiles with jets (shown in blue). In accordance with the spanwise modulation of the flow, the two profiles with jets represent the two extremes of the AJVG effectiveness: L_{min} corresponds to the fullest profile, leading to the smallest local separation length, and L_{max} represents the profile with the largest velocity deficit, inducing the largest local separation length for the case with jets. It is remarked that all profiles are self-similar in the outer part of the boundary layer ($y/\delta_0 > 0.8$), confirming once more that the free-stream

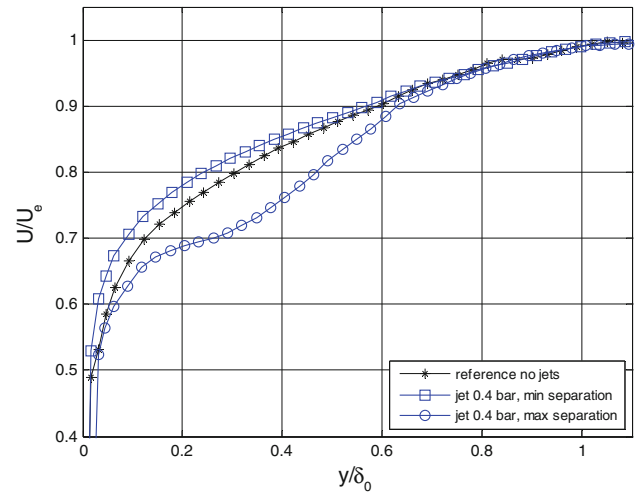


Fig. 8 longitudinal velocity profiles in the incoming boundary layer at $X = 260$ mm; black: reference profile without jets; blue: profiles with AJVGs control

velocity is not affected by the jets. It is noted that the jets cause a small but consistent increase in boundary layer thickness, see Table 2. The increase in velocity observed in Fig. 6 corresponds well to the increase in fullness of the boundary profile for L_{min} .

Using the rotation rate and the radius of the vortex, a vertical displacement of a fluid element can be deduced to examine the extent of the impact on the boundary layer profile. Given the radius of 3 mm for the CCW vortex and a rotation rate of $\alpha = 6.7 \times 10^3$ rad/s, the induced vertical displacement caused by the vortex rotation is estimated at 2 mm ($y/\delta_0 \approx 0.2$). Considering the reference boundary layer profile, such a displacement can indeed be held responsible for the change in fullness of the profiles with AJVGs and hence the modulation of the mean longitudinal velocity observed in Fig. 4 and in Fig. 6 at $Y = 1$ mm. This seems to confirm the mechanism proposed in Fig. 7.

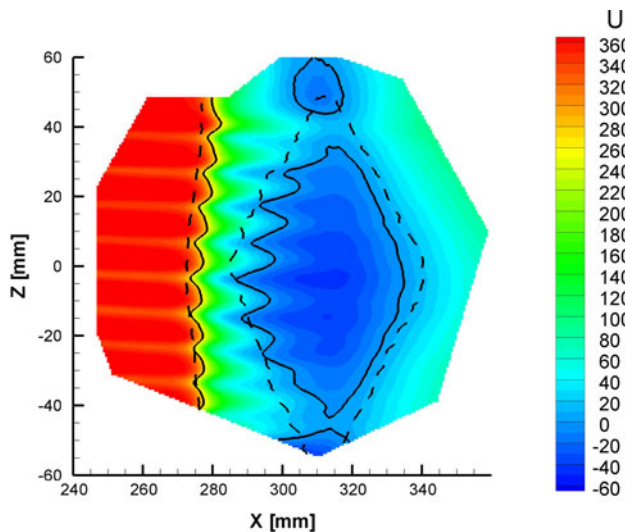
3.2 Modification of the separation bubble

The effect of injection on the mean flow topology has been investigated. The mean streamwise velocity component in the wall parallel plane at $Y = 1$ mm is shown in Fig. 9 for the case with or without control. The solid black contour lines in this figure indicate the streamwise velocity for 200 m/s (taken as indicative for the extrapolated reflected shock foot location) and for 0 m/s (representing the detachment line and the reattachment line and hence the extent of the separation bubble). The dashed lines indicate for reference the respective contours for the case without jets.

It was found that the 200 m/s velocity contour at the reflected shock foot location becomes rippled by the jets,

Table 2 Boundary layer parameters

	AJVG off	AJVG on				
	Ref.	Mean	Z = 2.5 mm (L_{\min})	Z = 0 mm	Z = -2.5 mm (L_{\max})	Z = 5 mm
δ_0 (mm)	9.9	10.4	10.1	10.5	10.3	10.6
δ^* (mm)	2.94	3.24	2.86	3.19	3.67	3.24
θ (mm)	0.84	0.91	0.84	0.92	0.98	0.89
H	3.52	3.56	3.42	3.46	3.75	3.64
C_f	2.09×10^{-3}	2.09×10^{-3}	2.30×10^{-3}	2.24×10^{-3}	1.81×10^{-3}	2.02×10^{-3}

**Fig. 9** Map of mean longitudinal velocity component (m/s) with AJVG control, $Y = 1$ mm

but that its mean spanwise position is only mildly affected, being pushed only slightly downstream when compared to the baseline interaction. This is in accordance with the thickening of the reflected shock observed in Fig. 2. The effect on the shock is small in comparison with the significant modifications in the upstream boundary layer that have been put into evidence above. Considering the separation bubble, it is clear that the separation line becomes highly corrugated in the injection case. This effect is more pronounced than the corrugation of the reflected shock. The reattachment line is displaced upstream with respect to the undisturbed case, but it shows no signs of corrugation. Hence, the effect of the jets is to decrease the separation length at each spanwise location.

As a general remark, it is observed that although clear traces of AJVG induced longitudinal vortices exist upstream of the separation bubble, no trace of such vortices is found downstream of the interaction: the reattachment line is uncorrugated, and no sign of the vortex-patterns is visible downstream of the reattachment. So either the longitudinal vortices are lifted over the interaction by the

separation bubble and do not reappear at a height of 1 mm, or they are destroyed by the unsteady processes occurring in the interaction region. These general observations in the plane at 1 mm from the wall are confirmed by visualisations obtained from the PIV-seeding deposit on the wall. The position of these deposit lines and their spanwise modulation are in accordance with the topology previously described using velocity at $y = 1$ mm. The experiments of Yamagata et al. 2009, who consider the control of the reattachment of a separated shear layer behind a backwards facing step at low subsonic conditions, would support the first hypothesis. They observe that the longitudinal vortices affect only the upper portion of the shear layer, while the lower portion remains unaffected. As a result, the reattachment line remains quasi-two dimensional in the spanwise direction. Such behaviour appears to be confirmed by the numerical results from Lee and Loth 2009, which indicate that the longitudinal vortex pairs are also lifted over the separation region.

As was shown in the previous section, the AJVGs appear to induce longitudinal vortices that entrain high-speed fluid from higher up in the boundary layer. This fluid slightly displaces the reflected shock foot downstream and reduces the separation length. The effect on the separation line is more pronounced than the effect on the reflected shock. To quantify this effect, Fig. 10 shows the velocity distribution at $Y = 1$ mm for L_{ref} , L_{min} and L_{max} .

As can be observed, the reattachment point with AJVGs is moved upstream when compared to the reference case. Furthermore, the separation point is moved downstream for L_{min} , while it is identical for L_{max} and L_{ref} . Hence, the separation length for L_{min} is significantly smaller than for L_{ref} , while L_{max} is only slightly smaller than L_{ref} . Downstream of the interaction, all cases attain the same mean velocity, and the effect of the jets hence disappears completely. The dip in the velocity in the upstream boundary layer indicates the location of the jet array. As can be seen, the velocity for L_{min} increases slightly between the jets and the separation region, while the velocity for L_{max} decreases. This is due to the slight skewing of the flow by the action of the jets, as observed previously, while the velocity distributions have been obtained in planes parallel

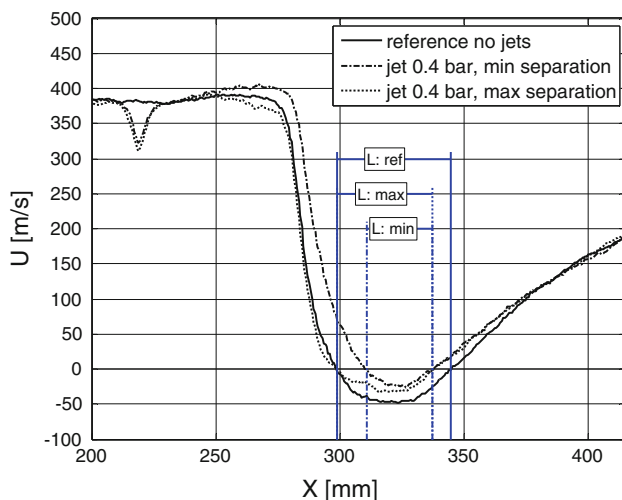


Fig. 10 Longitudinal distribution of mean longitudinal velocity component (m/s) with AJVG control, $Y = 1$ mm

to the tunnel axis. In addition to reducing the separation length, the AJVGs also reduce the separation bubble height, as has been observed in Fig. 3, with the largest reduction corresponding to the smallest separation length. The jets cause an overall decrease in separation length and an accompanying decrease in maximum reverse flow velocity.

An overview of the boundary layer parameters (with and without AJVGs) is given in Table 2. It shows the ability of the jets to affect the shock wave boundary layer interaction in a quantitative sense. The spanwise modulation of the boundary layer with jets is represented by four sections ($z = 2.5$ to -5 mm), corresponding to approximately one wavelength. ‘Mean’ signifies the approximate average

value, taken over these four spanwise sections. All quantities have been determined just upstream of the reflected shock foot. It has been verified that the values upstream of the interaction without jets (‘Ref.’) are practically identical to the values ahead of the jets array ($5\delta_0$ farther upstream). The compressible displacement and momentum thicknesses have been determined using the Crocco-Busemann relation. Overall, the action of the jets is to modulate the boundary layer parameters and to reduce the separation bubble size.

Concerning the effectiveness of the AJVGs to control the interaction, it is observed that similar results have been obtained in literature with other types of vortex generator devices (such as micro-vanes and micro-ramps), see for example Bruce and Babinsky (2008), Bur et al. (2009) and Lee and Loth (2009). The advantage of the AJVGs with respect to these control methods is that they can be easily turned off. In addition, one can envisage using AJVGs in combination with cooling approaches.

3.3 Modification of the shock dynamics

The intermittency in the shock position had been detected in the free stream using hot wire. The RMS values of the HWA signal induced by the passage of the shock are presented in Fig. 11 (left side) for different longitudinal positions with and without AJVG control. The maximum value of the RMS can be associated with the median shock location. A downstream shift in this location can be observed for the AJVG control case. This confirms the fact that the interaction length is slightly reduced with AJVG control; however, the shock excursion amplitude L_{ex} (indicated by the width of the peak) is not significantly

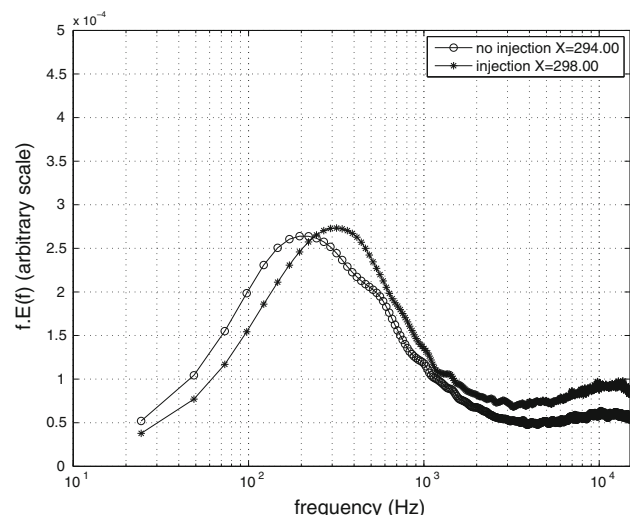
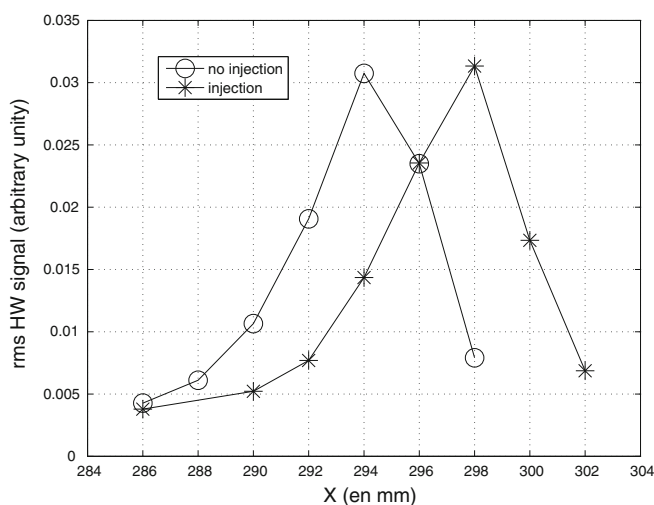


Fig. 11 Shock position and frequency measurements (circles: AJVGs off, asterisks: AJVGs on); left: RMS of the HWA signal for different positions with and without AJVG control; right: Pre-multiplied HWA spectrum for the reflected shock with and without jets

altered. The observed thickening of the shock in Fig. 2 can therefore not be attributed to an increased shock excursion length.

The shock frequency range has been detected in the free stream using a hot wire positioned at the median position of the separation shock. The resulting spectra of the HWA signal for the cases with and without injection is shown on the right side of Fig. 11. The spectrum is shown in pre-multiplied form ($fE(f)$ versus $\log(f)$, where f is the frequency) to correctly represent the energy concentration. The zone of the maximum spectral energy is not well defined but a significant shift in the peak energy of the spectrum to higher frequencies can be noticed when the jets are activated. This is in agreement with a quasi constant Strouhal number for the shock frequency (see Piponniau et al. 2009):

$$S_t = \frac{fh}{U}$$

where h is defined as the maximum height of the dividing streamline.

This can be demonstrated as follows. To determine the effect of the observed change in bubble height and shock frequency at constant reference velocity on the Strouhal number, one can write (using central differencing):

$$\frac{2\Delta S_t}{S_{t_0} + S_t} = \frac{2\Delta h}{h_0 + h} + \frac{2\Delta f}{f_0 + f}$$

The maximum height of the dividing streamline was found to be respectively $h_0 = 7.4$ mm for the reference case, and an average height of $h = 5.0$ mm for the case with jets ($h_{\max} = 5.7$ mm for L_{\max} and $h_{\min} = 4.2$ mm for L_{\min}). Referring to Fig. 11 (right side), the frequency is respectively $f_0 = 200$ Hz for the case without AJVGs and approximately $f = 300$ Hz with AJVGs. This leads to a negligible variation of the Strouhal number (approximately 1%) compared to a significant change in height and frequency (both about 40%). Such a modification of the frequency should be taken into account for practical control applications.

4 Conclusions

The results show the ability of the air jet vortex generators (AJVGs) to affect the shock wave boundary layer interaction in a quantitative sense. The principal effect of the AJVGs seems to be the modification of the mean velocity profile and the integral parameters of the inflow boundary layer, inducing a change in the separation bubble size.

The AJVGs, which are inclined at 45° with respect to the wall and blow in the transverse direction, generate a pair of longitudinal counter-rotating vortices per air jet.

The vortices are of unequal strength, with the stronger vortex located above the jet and the weaker vortex between the jet and the wall. The rotation rate of these vortices is small, notwithstanding the significant injection pressure and an important modification of the upstream boundary layer structure. Consequently, only a limited amount of mixing should be expected. However, it has been shown that the angular displacement induced by the flow is sufficiently large to entrain high-speed flow towards the wall, hence locally increasing the fullness of the boundary layer profile. At the same time, the opposite effect is observed in the wake of the jets, where the fullness is decreased. No significant effect has been observed of the AJVGs on the shock excursion amplitude and position. Moreover, the reattachment line is not corrugated, and no trace of the jets is observed after reattachment. However, the modification of the mean inflow boundary layer through this means of static control does reduce the separation bubble size without suppressing it.

As a direct consequence of the reduction in bubble size, the shock frequency is increased by about 50%. This behaviour is in agreement with the property that the Strouhal number for the shock frequency is constant: a higher frequency corresponds to a smaller separation bubble size, at least in the case of a well-developed mean separation bubble. We recall that the current reduction in the size of the separation bubble is obtained by means of static control: without considering unsteady effects in the inflow boundary layer, it appears that there is a direct link between the shock frequency and the mean bubble size.

Acknowledgments This work was carried out with support from a grant of the European STREP UFAST. Their support is gratefully acknowledged.

Open Access This article is distributed under the terms of the Creative Commons Attribution Noncommercial License which permits any noncommercial use, distribution, and reproduction in any medium, provided the original author(s) and source are credited.

References

- Andreopoulos J, Rodi W (1984) Experimental investigation of jets in crossflow. *J Fluid Mech* 138:93–127
- Ashill PR, Fulker JL, Hackett KC (2001) Research at DERA on sub boundary layer vortex generators (SBVGs). AIAA paper 2001-0887, Reno, Nevada
- Beresh SJ, Clemens NT, Dolling DS (2002) Relationship between upstream turbulent boundary layer velocity fluctuations and separated shock unsteadiness. *AIAA J* 40(12):2412–2422
- Blinde PL, Humble RA, Van Oudheusden BW, Scarano F (2009) Effect of micro-ramps on a shock wave/turbulent boundary layer interaction. *Shock Waves* 19(6):507–520
- Broadwell JE, Breidenthal RE (1984) Structure and mixing of a transverse jet in incompressible flow. *J Fluid Mech* 148:405–412

- Bruce PJK, Babinsky H (2008) Unsteady normal shock wave boundary layer interactions with control. AIAA paper 2008-721, Reno, Nevada, USA
- Bueno PC, Hou YX, Clemens NT, Dolling DS (2003) A PIV study on the effect of pulsed-jet injection upstream of a Mach 2 shock wave/boundary layer interaction. In: Proceedings of the 20th international congress on instrumentation in aerospace simulation facilities, Göttingen, Germany
- Bueno PC, Wagner JL, Searcy JA, Ganapathisubramani B, Clemens NT, Dolling DS (2006) Experiments in unsteady forcing of Mach 2 shock wave/boundary layer interactions. AIAA paper 2006-0878, Reno, Nevada, USA
- Bur R, Corbel B, Détery JM (1997) Study of passive control in a transonic shock wave/boundary layer interaction. AIAA paper 1997-0217, Reno, Nevada, USA
- Bur R, Coponet D, Carpels Y (2009) Separation control by vortex generator devices in a transonic channel flow. *Shock Waves* 19(6):521–530
- Cortezzi L, Karagozian AR (2001) On the formation of the counter-rotating vortex pair in transverse jets. *J Fluid Mech* 446:347–373
- Détery JM (2000) A physical introduction to control techniques applied to turbulent separated flows. AIAA paper 2000–2606, Denver, Colorado, USA
- Doerffer PP, Szluc O (2002) Shock wave strength reduction by passive control using perforated plates. *J Therm Sci* 16(2):97–104
- Dolling DS (2001) Fifty years of shock-wave/boundary-layer interaction research: what next? *AIAA J* 39(8):1517–1531
- Dupont P, Haddad C, Ardissonne JP, Debiève JF (2005) Space and time organisation of a shock wave/turbulent boundary layer interaction. *Aerosp Sci Technol* 9:561–572
- Dupont P, Haddad C, Debiève JF (2006) Space and time organization in a shock induced boundary layer. *J Fluid Mech* 559:255–277
- Dupont P, Piponniau S, Sidorenko A, Debiève JF (2008) Investigation of an oblique shock reflection with separation by PIV measurements. *AIAA J* 46(6):1365–1370
- Dussauge JP, Piponniau S (2008) Shock/boundary-layer interactions: possible sources of unsteadiness. *J Fluids Struct* 24:1166–1175
- Dussauge JP, Dupont P, Debiève JF (2006) Unsteadiness in shock wave boundary layer interactions with separation. *Aerosp Sci Technol* 10:85–91
- Elena M, Tedeschi G, Gouin H (1999) Motion of tracer particles in supersonic flows. *Exp Fluids* 26(4):288–296
- Fric TF, Roshko A (1994) Vortical structure in the wake of a transverse jet. *J Fluid Mech* 279:1–47
- Ganapathisubramani B, Clemens NT, Dolling DS (2007) Effects of upstream on the unsteadiness of shock induced separation. *J Fluid Mech* 585:369–394
- Green JE (1970) Interactions between shock waves and turbulent boundary layers. *Prog Aerosp Sci* 11:235–340
- Holden H, Babinsky H (2007) Effect of microvortex generators on separated normal shock/boundary layer interactions. *J Aircraft* 44(1):170–174
- Humble RA, Elsinga GE, Scarano F, Van Oudheusden BW (2009) Three-dimensional instantaneous structure of a shock wave/turbulent boundary layer interaction. *J Fluid Mech* 622:33–62
- Kamotani Y, Greber I (1972) Experiments on a turbulent jet in a cross flow. *AIAA J* 10(11):1425–1429
- Lee S, Loth E (2009) Supersonic boundary layer interactions with various micro-vortex generator geometries. AIAA paper 2009-3712, San Antonio, Texas, USA
- Lee S, Loth E, Georgiadis NJ, DeBonis JR (2009) Effect of Mach number on flow past micro-ramps. AIAA paper 2009-4181, San Antonio, Texas, USA
- Lin JC (2002) Review of research on low-profile vortex generators to control boundary-layer separation. *Prog Aerosp Sci* 38:389–420
- Piponniau S, Dussauge JP, Debiève JF, Dupont P (2009) A simple model for low-frequency unsteadiness in shock-induced separation. *J Fluid Mech* 629:87–108
- Scarano F, Riethmuller ML (1999) Iterative multigrid approach in PIV image processing with discrete window offset. *Exp Fluids* 26:513–523
- Selig MS, Smits AJ (1991) Effect of periodic blowing on attached and separated supersonic turbulent boundary layers. *AIAA J* 29(10):1651–1658
- Smith SH, Mungal MG (1998) Mixing, structure and scaling of the jet in crossflow. *J Fluid Mech* 357:83–122
- Souverain LJ, Debiève JF, Dupont P, Dussauge JP (2008) Control of an Incident shock wave/turbulent BL interaction, $M = 2.3$ by means of Air Jet Vortex Generators. UFAST Deliverable 3.3.3
- Souverain LJ, Dupont P, Debiève JF, Dussauge JP, Van Oudheusden BW, Scarano F (2009) Effect of interaction strength on shock wave boundary layer interaction: unsteady behavior. AIAA paper 2009-3715, San Antonio, Texas, USA
- Valdivia A, Yuceil KB, Wagner JL, Clemens NT, Dolling DS (2009) Active control of supersonic inlet unstart using vortex generator jets. AIAA paper 2009-4022, San Antonio, Texas, USA
- Viswanath PR (1988) Shock-wave-turbulent-boundary-layer interaction and its control: a survey of recent developments. *Sadhana* 12:45–104
- Yamagata K, Morioka T, Motosuke M, Honami S (2009) A role of longitudinal vortex on the separating shear layer development over a backward facing step. AIAA paper 2009-4180, San Antonio
- Yang YT, Wang YX (2005) Three-dimensional numerical simulation of an inclined jet with cross-flow. *Int J Heat Mass Transf* 48:4019–4027